THE ASTROPHYSICAL JOURNAL, 369:L27–L30, 1991 March 10

HST IMAGING OF THE INNER 3 ARCSECONDS OF NGC 1068 IN THE LIGHT OF [O III] λ5007

I. N. EVANS,[1] H. C. FORD,[2,3] A. L. KINNEY,[1] R. R. J. ANTONUCCI,[4] L. ARMUS,[2] AND S. CAGANOFF[2]
Received 1990 October 8; accepted 1990 December 4

ABSTRACT

We have used the Planetary Camera on board the *Hubble Space Telescope* to obtain a high spatial resolution [O III] λ5007 image of the nucleus of NGC 1068. This image resolves the narrow-line region into several distinct clouds arranged in an apparently conical geometry. The individual emission-line regions appear to be resolved, with sizes ~0".1–0".2 (~6–12h pc; $H_0 = 100h^{-1}$ km s^{-1} Mpc^{-1}). There is a strong apparent correspondence between the 1.3 cm radio "triple" structure and several of the [O III] λ5007 clouds, although there are also bright emission-line clouds for which there are no radio counterparts. Based on the combined [O III] λ5007 and radio continuum morphology, we conclude that the hidden nucleus is located in the southern radio component, together with the H_2O megamaser.

Subject headings: galaxies: individual (NGC 1068) — galaxies: nuclei — galaxies: Seyfert

1. INTRODUCTION

The unusual emission-line spectrum of the barred spiral galaxy NGC 1068 was first noted by Fath in 1909; see Osterbrock (1990) for an excellent review of active galactic nuclei. Seyfert (1943) included NGC 1068 in a list of galaxies that have nuclei with bright, broad emission lines arising from relatively highly ionized elements. NGC 1068 has since been classified as a Seyfert 2 and is the nearest and brightest luminous example of this kind of galaxy; both the permitted and forbidden lines in Seyfert galaxies are broadened by a few hundred km s^{-1}, whereas the permitted lines in Seyfert 1 galaxies also have a component which is broadened by several thousand km s^{-1}. Antonucci & Miller (1985) detected a featureless continuum and broad permitted lines in polarized light from the nuclear region of NGC 1068 and concluded that in light reflected by electron scattering they were observing the spectrum of a bright Seyfert 1 nucleus which is obscured by a very thick absorbing disk. Pogge (1988) used excitation maps to show that the ionizing radiation from the hidden nucleus is observable in a one-sided cone. Miller & Goodrich (1990) made spectropolarimetric measurements of eight other Seyfert 2 galaxies and found that at least four of them show the signature of a hidden Seyfert 1 nucleus. In a survey of 11 Seyfert 2 galaxies, Pogge (1989) found evidence for ionization cones in three additional galaxies.

In this *Letter*, we report the first *Hubble Space Telescope* (*HST*) narrow-band image of NGC 1068. This image, which was taken directly from the Faint Object Spectrograph (FOS) Investigation Definition Team (IDT) program, was executed as part of the Science Assessment Observations.

2. OBSERVATIONS AND REDUCTIONS

The data were gathered using the Planetary Camera (PC) configuration of the Wide-Field/Planetary Camera (WFPC) on board *HST* on 1990 August 26. One exposure was obtained in each of the filters (narrow-band [O III] λ5007, nominal mean wavelength/effective width 5019/30 Å) and F547M (off-band continuum, 5462/433 Å), with the nucleus of the galaxy located near the default pointing position on the CCD PC6. At the time of the observations, the CCDs were not UV-flooded. Exposure times for the on- and off-band frames were 900 and 180 s, respectively. During the observations, the spacecraft was maintained in coarse track without any losses of lock. The RMS pointing jitter was 51 mas for the on-band exposure, and 43 mas for the continuum frame.

The data were automatically processed by the WFPC Routine Science Data Processing pipeline at the Space Telescope Science Institute. The reductions applied to the data follow the precepts of Lauer (1989) which should be consulted for more information.

The calibration data employed during pipeline processing were those obtained prior to the launch of *HST*. The main source of uncertainty which arises from using the prelaunch calibration data results from changes in the intermediate scale structure in the flat fields due to dust and similar contamination of the WFPC optics. The large-scale structure of the flat fields is also uncertain because the prelaunch calibration data were obtained when the CCDs were UV-flooded. However, the pixel-to-pixel variations in the detector sensitivity are relatively well calibrated. Based on a comparison of on-orbit and ground-based flat fields obtained through the F547M filter, we estimate that the calibration accuracy of the processed data is no worse than ~10% in the region of the nucleus.

Following pipeline processing, the contribution of the continuum through the narrow-band filter was removed. Since the background level varied by ~30%–40% from the center to the corners of each frame, we adjusted the measured level of the 150 × 150 pixel area centered on the brightest [O III] λ5007 cloud by adding a constant value determined by scaling the average value measured in the corners of the image. A linear shift derived from a two-dimensional fit to stars visible through both filters was then applied to the off-band image to register it with the on-band image. The uncertainty in the alignment of the two frames is ~0.13 pixels (~5.5 mas). Finally, a scaled version of the shifted off-band image was subtracted from the on-band image. We empirically determined the scale factor by

[1] Space Telescope Science Institute, 3700 San Martin Drive, Baltimore, MD 21218.
[2] Johns Hopkins University, Department of Physics and Astronomy, Homewood Campus, Baltimore, MD 21218.
[3] Also Space Telescope Science Institute.
[4] University of California at Santa Barbara, Physics Department, Santa Barbara, CA 93106.

requiring that the stellar disk of NGC 1068 disappear in the resulting "pure" [O III] λ5007 image. The results of this method depend not only upon the color difference between the disk stars and the nuclear continuum source, but also upon the rather uncertain flat field correction discussed above. We estimate that the internal uncertainy in our measurement of the total nuclear [O III] λ5007 flux is ~10%.

Following continuum subtraction, a region of the narrow-band image centered on the nucleus was deconvolved using the maximum entropy method (MEM), to correct for the spatial blurring of the data caused by the spherical aberration present in the *HST* optics. We used the MEMSYS 3 software (Gull & Skilling 1989) to deconvolve the data.

The point-spread function (PSF) used to deconvolve the data was derived from PC images of the isolated star HD 124063 obtained through the F487N (4869/31 Å) filter made at the same telescope focus as the science observations. Although these frames were obtained through a different filter than the science observations, the variation of the PSF as a function of wavelength between these filters is negligible. A more serious problem is that HD 124063 was approximately centered on PC6, whereas the nucleus of NGC 1068 was located ~200 pixels away from the center of the CCD. This produces different internal vignetting in the PC for the star used to derive the PSF relative to the nucleus of NGC 1068, resulting in variations in the broad wings of the PSF at the level of several percent of the peak intensity. Because of the extreme difference in the intensity of the bright core of the PSF and the faint extended wings resulting from the spherical aberration, the final PSF was constructed by combining with appropriate scaling the core of the profile from a short exposure frame with the wings from a longer exposure in which the core was moderately saturated. This procedure effectively increases the dynamic range of the PSF, at the expense of some minor uncertainty in the position of the core relative to the centroid of the wings. However, since the frames from which the PSF was determined were obtained in one orbit without any loss of lock between the exposures, this error should be no worse than the RMS pointing jitter.

The deconvolution was performed using an essentially identical technique to the one described by Evans, Ford, & Hui (1989). The MEM solution was computed using estimated errors in the measured pixel intensities which included the uncertainties in the pipeline processing (such as flat-fielding errors) and the continuum subtraction process, as well as the contributions from readout noise and photon statistics. The original continuum-subtracted image of the nuclear regions is presented in Figure 1 (Plate L3), while the final MEM solutions are shown in Figures 2 and 3 (Plates L3 and L4). It can be estimated from the FWHM of the narrowest features in the reconstruction that the resolution is ~0.″085.

Reduction of the image to an astrometric reference frame was conducted using the Guide Star Catalog (GSC1) as the primary reference. Because of the small field of the PC6 frame, it was not possible to calibrate the image directly. Instead, the GSC1 was used to calibrate a red continuum CCD image of NGC 1068, and the latter was then used to derive an astrometric calibration for the PC6 continuum frame. A correction for the shift between the on- and off-band images was applied to the astrometric solution to derive the final astrometric calibration for the continuum-subtracted [O III] λ5007 image. The formal accuracy of the astrometric calibration in the GSC1 reference frame is 0.″2. We derive a plate scale of 0.″0421 pixel^{-1} for our PC frames.

We were able to compute an approximate photometric calibration for the frame by using the XCAL package (Horne 1990). From the deconvolved image, we derive a nuclear [O III] λ5007 flux of 1.54×10^{-11} ergs cm^{-2} s^{-1} in a 4.″0 × 2.″7 area oriented north-south centered on the brightest [O III] λ5007 cloud. This flux is approximately 74% of the flux measured from the ground through a similar aperture by Koski (1978). The broad wings seen in the [O III] λ5007 profiles measured by Alloin et al. (1983) indicate that ~10%–15% of the line flux may have fallen outside of the *nominal* bandpass of the F502N filter, redward of the line center. However, the transmission curves of the WFPC filters have not been measured for approximately a decade, and so the throughput and bandpass of the F502N may have changd during this time. Changes in the median wavelength of the transmission curve may have shifted high-velocity features completely out of the effective filter bandpass. We estimate that the uncertainty in our PC flux calibration is ~10%–15%, which is comparable to the discrepancy between the total flux measured by Koski (1978) and the value derived from our [O III] λ5007 image. A contour plot of the astrometrically and approximately photometrically calibrated deconvolved image is presented in Figure 4.

3. DISCUSSION

Inspection of the figures reveals the presence of many [O III] λ5007 emission-line regions. For future reference, we have identified the principal of these in Figure 2. It can clearly be seen that some of these regions are extended on scales of ~0.″1–0.″2 (~6–12h pc; $H_0 = 100h^{-1}$ km s^{-1} Mpc^{-1}), indicating that they are either themselves spatially resolved, or that the extensions are the result of a near superposition of more than one emitting cloud. The morphology of region C is reminiscent of a bow shock resulting from the interaction of the radio jet with the interstellar medium (ISM), although the axis of symmetry of this region does not obviously point along the radio jet toward the most probable location of the nucleus (see below). On the basis of the 2 and 6 cm radio morphology, Wilson & Ulvestad (1987) have suggested that a radiative bow shock resulting from compression of the ISM by the radio jet may be present in the flow at a distance of ~13″ from the nucleus.

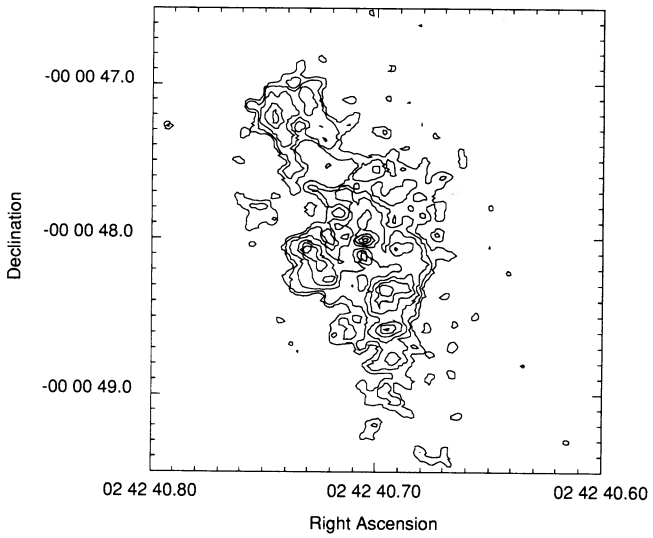

FIG. 4.—Contour plot of the reconstruction presented in Fig. 3. The contour levels are 0.25, 0.5, 1, 2, 3, 4, and 5×10^{-12} ergs cm^{-2} s^{-1} arcsec^{-1}.

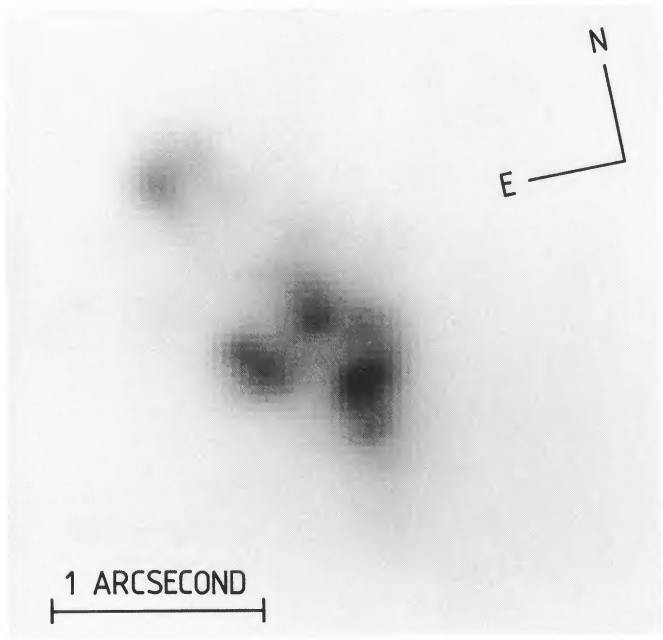

FIG. 1

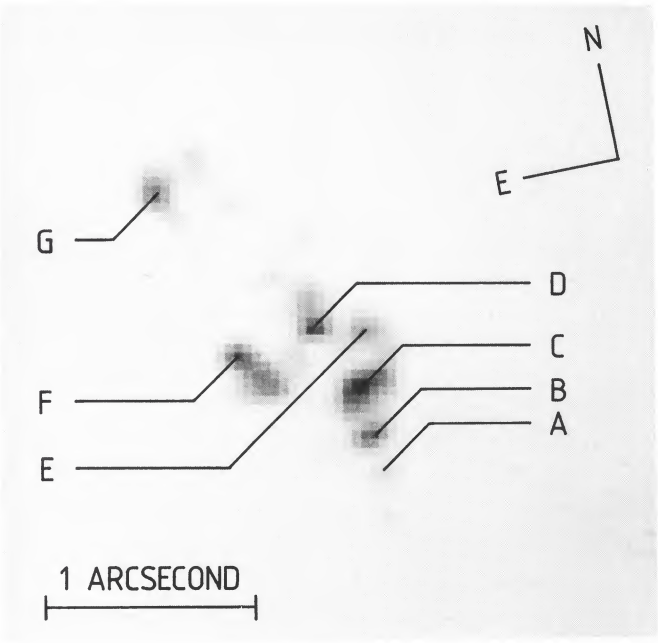

FIG. 2*a*

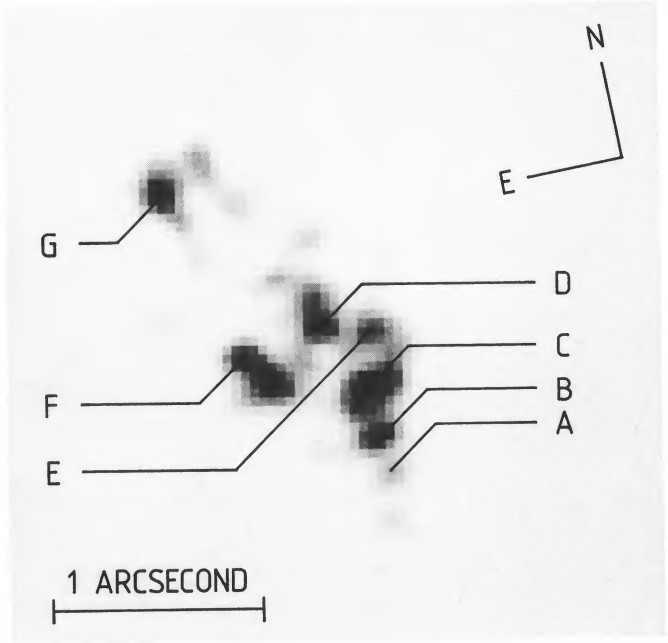

FIG. 2*b*

FIG. 1.—Continuum-subtracted [O III] λ5007 image of the nucleus. The image intensity is linearly scaled.

FIG. 2.—MEM reconstruction of Fig. 1, sampled at the same pixel spacing as that figure. Clouds A–G are indicated. The image on the left is scaled from 5% to 100% of the peak intensity, while the image on the right is scaled between 5% and 50% of the peak intensity to display the faint details in the reconstruction.

EVANS et al. (see 369, L28)

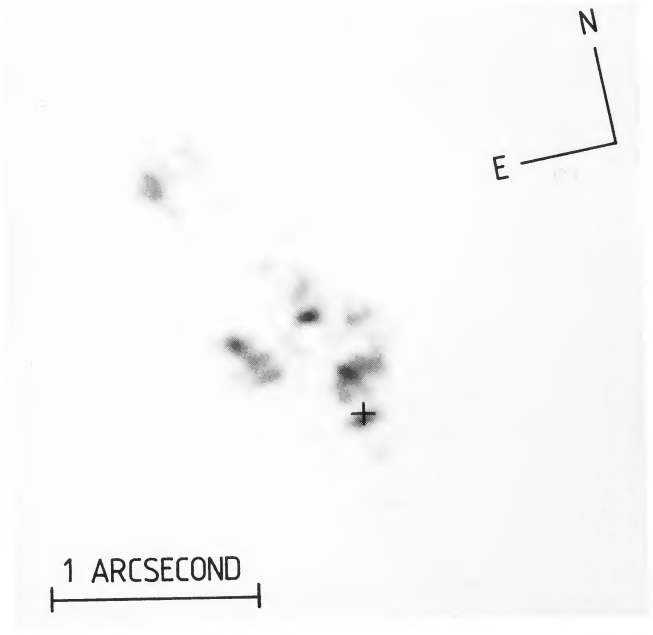

FIG. 3*a*

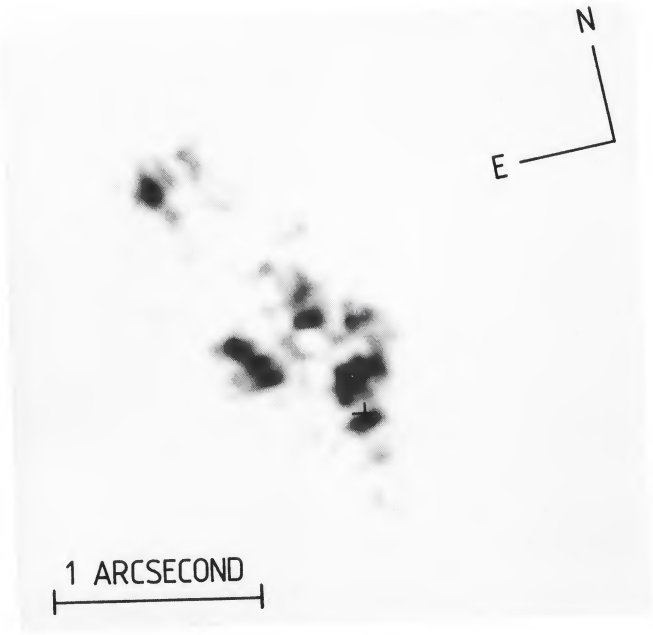

FIG. 3*b*

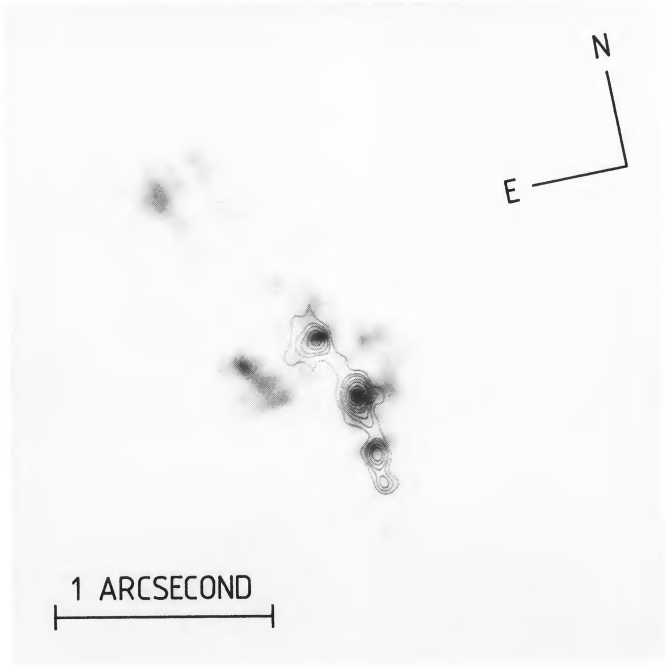

FIG. 5

FIG. 3.—As Fig. 2, except that the reconstruction is sampled at 4 times the pixel sampling of that figure. This produces a smoother looking deconvolved image. The position of the continuum peak is marked.

FIG. 5.—As Fig. 3, except that our preferred registration of the 1.3 cm radio map of Ulvestad et al. (1987) is overlaid in the form of a contour plot

The distribution of the [O III] λ5007 emission is highly suggestive, forming an apparently conical geometry in the plane of the sky. The position of the apex of the cone is very difficult to determine accurately from the data, since the derived location is strongly dependent on the flux level. Nevertheless, it seems highly improbable that the apex lies north of cloud B, or more than ~0".4 south of cloud A. Given the uncertainty in the position of the apex, we derive a cone opening angle projected on the plane of the sky of 65° ± 20° with a P.A. of ~15°. The larger opening angles are associated with cones which have their apex near cloud B. The projected cone opening angle derived here is in good agreement with the results of Bergeron, Petitjean, & Durret (1989), Pogge (1989), and Cecil, Bland, & Tully (1990), who derive values of ~40°–80° from observations of emission-line material at greater distances from the nucleus. These authors derive a cone P.A. of ~30°–35°, however, from ground-based data. If this geometry arises as a result of illumination of these narrow-line clouds by photoionizing radiation directly beamed from the active nucleus, then the nucleus of NGC 1068 must be located approximately at the position of the apex of the cone. This implies that the bright peak visible in the continuum frame (Lynds et al. 1991) is *not* coincident with the nucleus, since it is located ~50 mas (~3*h* pc) north of cloud B, as indicated in Figure 3.

High-resolution ground-based [O III] λ5007 images of NGC 1068 were obtained by Ebstein, Carleton, & Papaliolios (1989) and Hoffman, Mauder, & Weigelt (1989), using various speckle imaging techniques. These images have [O III] λ5007 emission extended generally at the correct position angle, but with differences in the relative positions and fluxes of the components when compared to the *HST* image. Both papers report a weak component which is not detected in the *HST* image, ~0".5 south of cloud C, but the images do not resolve clouds A and B. Although their extra component may arise from high-velocity [O III] λ5007 emission which is not seen in the PC images obtained through the narrow F502N filter, it is not visible in higher quality follow-up speckle images obtained by Weigelt (1990) and is probably spurious. The speckle images are not sensitive to as broad a dynamic range as the *HST* images.

The four emission-line clouds, A–D, bear a striking morphological similarity to the four components of the 1.3 cm radio map published by Ulvestad, Neff, & Wilson (1987). The separations of the [O III] λ5007 clouds and the radio sources are very similar in distance and position angle, although they are not identical. Slight displacement between emission-line knots and associated radio knots has been noted in other Seyfert galaxies (e.g., Whittle et al. 1986; Pedlar, Dyson, & Unger 1985). We prefer to register the 1.3 cm radio map and the optical emission-line data as shown in Figure 5 (Plate L4) (in which the radio map has been precessed to J2000 coordinates and the position angles and scales of the two sets of data are identical), and we will assume this alignment throughout the rest of this *Letter*. The two components of the southern radio hot spot then correspond to clouds A and B, while the brightest radio hot spot corresponds to cloud C, the brightest [O III] λ5007 emission-line region. Beyond cloud C, the radio jet bends to the northeast, passing through cloud D where we find another radio hot spot, and then continues to the northeast where it feeds a large wedge-shaped radio lobe (Wilson & Ulvestad 1983). The emission-line cloud G is coincident with an enhancement of the radio jet close to the base of the lobe and is probably identified with the northeast source of 10 μm emission identified by Tresch-Fienberg et al. (1987), which may be a region of active star formation induced by interaction of the radio jet with the ISM. To achieve our preferred registration between the 1.3 cm radio and optical images, it is necessary to offset the published radio coordinates by ~0".7. This offset is similar to the sum in quadrature of the uncertainty in our PC astrometry (~0".2), the local astrometric uncertainties between the GSC1 and VLBI reference frames (~0".6; Russell et al. 1990), and the positional uncertainty of the radio observations due to phase errors (~0".3 for the 1.3 cm observation of Ulvestad et al. 1987), and is therefore adequately explained by the astrometric uncertainties of the observations. The spatial correlation between radio hot spots and emission-line knots presents an appealing scenario of interaction between the jet and the emission-line clouds which would be much less plausible if the relative positions of the optical and radio maps were to be displaced even by as little as ~0".1.

It is particularly interesting to note that neither of the emission-line clouds E or F appears to have associated radio emission. This may be explained directly by differences in the excitation mechanisms of these clouds, or it may suggest that the [O III] λ5007 emission is not causally related to the radio jet (possibly implying that the mechanical energy imparted by the interaction of the jet with the ISM is small compared to the energy provided by the photoionizing radiation). Additional FOS observations are required to distinguish between possible scenarios.

If the active nucleus of NGC 1068 lies at the apex of the apparently conical emission line region, then our registration of the radio and optical images implies that the true nucleus lies to the south of the central radio component and at or near the location of the southern component of the "triple" radio source. If this is correct, then the nucleus is not the strongest radio source. However, this is known to be the case for many Seyfert nuclei (e.g., Ulvestad & Wilson 1984).

Such a placement for the nucleus suggests that the nuclear H_2O megamaser may be identified with the dusty torus invoked to block our direct view of the optical continuum and the broad line region (Antonucci & Miller 1985), in agreement with the assertion of Claussen & Lo (1986). These authors were confident that the megamaser is truly associated with the active nucleus because of the ~600 km s^{-1} velocity width of the line, the compactness of the source, and the extreme physical conditions required to produce such a large maser luminosity. Since the megamaser definitely corresponds to the *southernmost* member of the inner radio triple, Claussen & Lo (1986) conclude that that component must be the true nucleus. The southern radio component is itself actually double, with [O III] λ5007 clouds associated with each subcomponent. Tentatively, the published data suggest that the maser may be identified with the *northern* subcomponent (Claussen 1990). If the location of the H_2O megamaser is truly coincident with active nucleus and, therefore, with the apex of the ionizing cone, then emission-line cloud A must be located on the side of the nucleus *opposite* to the main ionizing cone.

On the other hand, Ulvestad et al. (1987) have suggested that the central radio component of the "triple" is the true nucleus, since it appears to be the most compact and may have a relatively flat radio spectrum. However, the compactness and flatness arguments are weakened by problems with different sensitivities to different spatial scales of the multifrequency maps. In particular, these arguments rely on a 21 cm European VLBI Network (EVN) map (see Fig. 3 of Ulvestad et al. 1987),

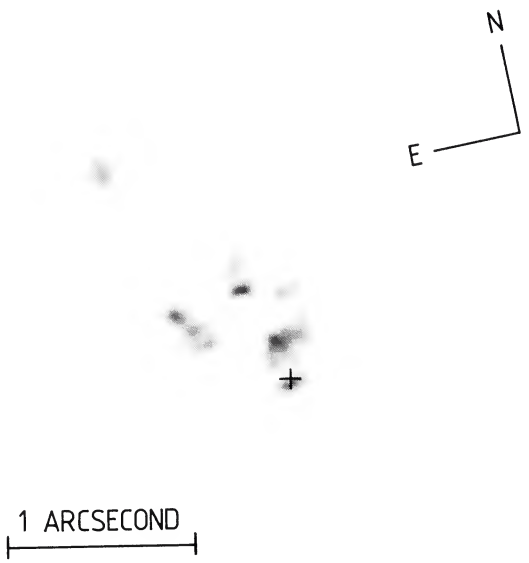

FIG. 3*a*

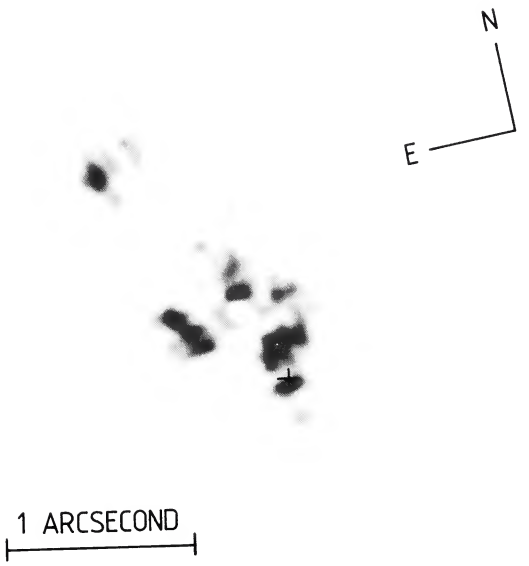

FIG. 3*b*

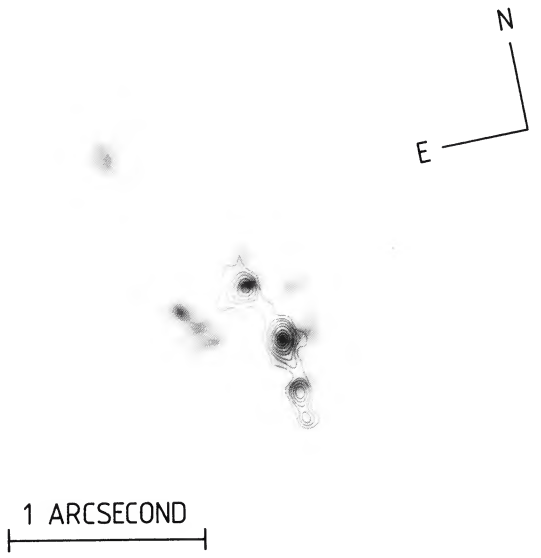

FIG. 5

FIG. 3.—As Fig. 2, except that the reconstruction is sampled at 4 times the pixel sampling of that figure. This produces a smoother looking deconvolved image. The position of the continuum peak is marked.

FIG. 5.—As Fig. 3, except that our preferred registration of the 1.3 cm radio map of Ulvestad et al. (1987) is overlaid in the form of a contour plot

and the identification of its three apparent components with the three definite components of the VLA 1.3 and 2 cm maps. The EVN map shows two weak hot spots placed almost exactly symmetrically about a stronger source. Such symmetry suggests possible spurious features due to amplitude errors in the data. More importantly, if the strongest EVN component is identified with the strongest VLA component, as argued by Ulvestad et al. (1987), then the southern component does not agree well positionally with the southern component on the VLA maps. In other words, the definite southern VLA component detected at high frequencies may well be absent or weak at 21 cm. If that is the case, then the southern radio component actually has a steeply rising spectrum.

Weakness or absence of the southern radio component at 21 cm is naturally explained by the torus model of Krolik & Lepp (1989). They assume that the molecular torus must have a very high column density ($\gtrsim 10^{24}$ cm^{-2}, based on the blocking of hard X-rays and broad Brackett-alpha emission) and that it is illuminated by a Seyfert 1 type X-ray source. It then follows that the low cm radio frequencies *must be free-free absorbed.* For their nominal parameters, Krolik & Lepp (1989) predict that the nucleus must be absorbed below 10 GHz (3 cm). This seems to be impossible for the central radio component (see Table 1 of Ulvestad et al. 1987) but might be exactly what the radio data imply about the southern component.

Since the radio "triple" is bent, locating the nucleus near the southern radio component also enhances the claim of Antonucci (1983) that the optical polarization position angles of Seyfert 2 galaxies with intrinsic nuclear polarization are perpendicular to the radio jets, since the radio P.A. at this location is $\sim 10°$, which is almost exactly perpendicular to the optical polarization P.A. (95°; Miller & Antonucci 1983; Antonucci & Miller 1985).

Finally, Miller, Goodrich, & Mathews (1990) note that the relative narrowness of the permitted lines in polarized flux requirs that the reflecting electrons are relatively cool ($\lesssim 3 \times 10^5$ K), and that this is consistent with all of the other constraints only if the reflection region is located many pc from the nucleus. Qualitatively, this is consistent with the hypothesis that the nucleus is located in the southern radio component, since the optical continuum peak is displaced from it. (Assuming that the nucleus is coincident with the H_2O megamaser, the projected separation is ~ 90 mas, $\sim 5h$ pc, for our preferred registration of the optical and radio data).

4. SUMMARY AND CONCLUSIONS

We have used the PC aboard *HST* to obtain a high spatial resolution [O III] λ5007 image of the nucleus of NGC 1068. This image shows more detail than any previously published images and resolves the NLR into several distinct clouds arranged in an apparently conical geometry. Following MEM image deconvolution, we find that individual emission-line regions appear to be resolved, with sizes $\sim 0\farcs1$–$0\farcs2$ (~ 6–$12h$ pc). There is a strong apparent correspondence between the 1.3 cm radio structure and several of the [O III] λ5007 clouds, although there are also bright emission-line clouds for which there are no radio counterparts. In particular, the radio "triple" of Ulvestad et al. (1987) appears to correspond directly to the [O III] λ5007 clouds A–D. The peak in the optical continuum emission (Lynds et al. 1991) is located near, but not coincident with, cloud B.

We conclude the following:

1. The distribution of [O III] λ5007 clouds is consistent with ionization cone models.

2. Based on the combined [O III] λ5007 and radio continuum morphology, the hidden nucleus is located somewhere in the southern radio component and may be coincident with the H_2O megamaser.

3. The peak in the optical continuum is possibly a mirror illuminated by the hidden luminous nucleus.

The authors would like to acknowledge stimulating discussions with Hans-Martin Adorf, Mark Claussen, John Skilling, James Ulvestad, Gerd Weigelt, Nick Weir, and Andrew Wilson. Invaluable assistance in reducing the data was provided by Ralph Bohlin, Eric Deutsch, Keith Horne, and John MacKenty. This work was supported in part by NASA contract NAS 5-29293.

REFERENCES

Alloin, D., Pelat, D., Boksenberg, A., & Sargent, W. L. W. 1983, ApJ, 275, 493
Antonucci, R. R. J. 1983, Nature, 303, 158
Antonucci, R. R. J., & Miller, J. S. 1985, ApJ, 297, 621
Bergeron, J., Petitjean, P., & Durret, F. 1989, A&A, 213, 61
Cecil, G., Bland, J., & Tully, R. B. 1990, ApJ, 355, 70
Claussen, M. J. 1990, private communication
Claussen, M. J., & Lo, K.-Y. 1986, ApJ, 308, 592
Ebstein, S. M., Carleton, N. P., & Papaliolios, C. 1989, ApJ, 336, 103
Evans, I. N., Ford, H. C., & Hui, X. 1989, ApJ, 347, 68
Fath, E. A. 1909, Lick Obs. Bull., 5, 71
Gull, S. F., & Skilling, J. 1989, Quantified Maximum Entropy "MEMSYS 3" Users' Manual (Version 2.00; Royston: Maximum Entropy Data Consultants Ltd.)
Hoffman, K.-H., Mauder, W., & Weigelt, G. 1989, in Proc. ESO Workshop on Extranuclear Activity in Galaxies, ed. R. Fosbury & J. Meurs (Munich: European Southern Observatory), p. 35
Horne, K. 1990, XCAL Users Manual (Version 1.1; Baltimore: Space Telescope Science Institute)
Koski, A. T. 1978, ApJ, 223, 56
Krolik, J. H., & Lepp, S. 1989, ApJ, 347, 179
Lauer, T. R. 1989, PASP, 101, 445
Lynds, C. R., et al. 1991, ApJ, 369, L31
Miller, J. S., & Antonucci, R. R. J. 1983, ApJ, 271, L7
Miller, J. S., & Goodrich, R. W. 1990, ApJ, 355, 456
Miller, J. S., Goodrich, R. W., & Mathews, W. G. 1990, ApJ, submitted
Osterbrock, D. E. 1990, Rep. Prog. Phys., submitted
Pedlar, A., Dyson, J. E., & Unger, S. W. 1985, MNRAS, 214, 463
Pogge, R. W. 1988, ApJ, 328, 519
———. 1989, ApJ, 345, 730
Russell, J. L., Lasker, B. M., McLean, B. J., Sturch, C. R., & Jenkner, H. 1990, AJ, 99, 2059
Seyfert, C. K. 1943, ApJ, 97, 28
Tresch-Fienberg, R., Fazio, G. G., Gezari, D. Y., Hoffmann, W. F., Lamb, G. M., Shu, P. K., & McCreight, C. R. 1987, ApJ, 312, 542
Ulvestad, J. S., Neff, S. G., & Wilson, A. S. 1987, AJ, 93, 22
Ulvestad, J. S., & Wilson, A. S. 1984, ApJ, 278, 544
Weigelt, G. 1990, private communication
Whittle, M., Haniff, C. A., Ward, M. J., Meurs, E. J. A., Pedlar, A., Unger, S. W., Axon, D. J., & Harrison, B. A. 1986, MNRAS, 222, 189
Wilson, A. S., & Ulvestad, J. S. 1983, ApJ, 275, 8
———. 1987, ApJ, 319, 105